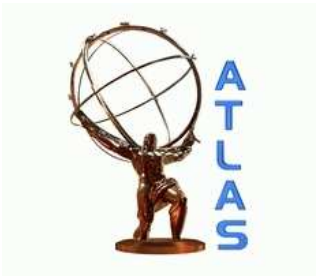

ATLAS NOTE

ATL-PHYS-PUB-2006-000

October 19, 2007

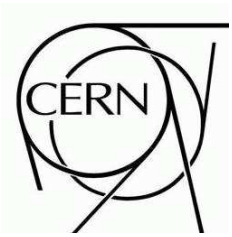

A pre-commissioning $t\bar{t}$ cross section measurement at ATLAS

The ATLAS Collaboration

Abstract

In this document we describe the measurement of the $t\bar{t}$ cross section in the electron + jets channel, using the inclusive electron streaming dataset. Using events passing the LVL2 25 GeV isolated electron trigger, we observe 486 $t\bar{t}$ candidate events with a tight electron and four central jets in the data. After correcting for electroweak, diboson, and single top background sources, we find that this corresponds to a $t\bar{t}$ cross section of FINAL RESULT. We also describe studies of the number of *b*-tagged events and events with a tight muon from the same trigger, which are consistent with the measured top cross section and could be used to refine the analysis.

1 Introduction

Motivation+Method

2 Event selection

We use the inclusive electron streaming dataset, generated from a mixture of physics processes simulated in release 11.0.42. The dataset corresponds to a nominal luminosity of 18 pb^{-1}, but the streaming event generation includes simulated online "dead-time" and some luminosity blocks of bad data. Using the prototype luminosity/conditions database [**?**] to account for deadtime corrections and file losses, the luminosity in the inclusive electron samples `streamtest.00*.inclEle.merge.AOD.v12000605` is 15.03 pb^{-1}. Removing the three luminosity blocks marked "BAD" in the database, we are left with 14.86 pb^{-1} of data for this analysis.

2.1 Cuts

This section describes our object-level cuts that define what we call an "electron" and a "jet"; then describes the event-level cuts that we use in this study.

Electron definition

Electron is an object from an `ElectronContainer` with the StoreGate key *ElectronCollection*, which satisfies:

1. AuthorEgamma,
2. $|eta| < 2.4$ and $|\eta| \notin [1.37, 1.52]$,
3. $p_T > 25$ GeV.

Distributions of the p_T and η cut variables are shown on Fig. 1.

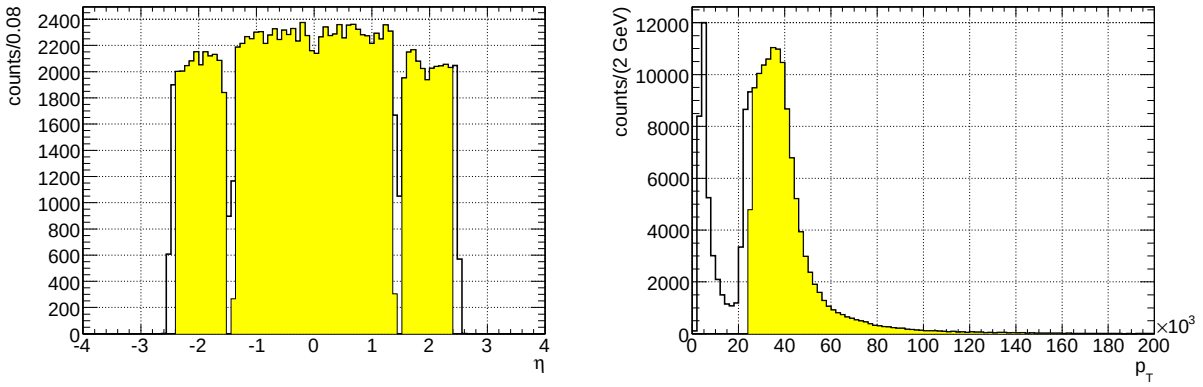

(a) (b)

Figure 1: Distributions of η (1(a)) and p_T (1(b)) of electron candidates. The η distribution includes only those the candidates that passed the p_T cut, and p_T distribution only the candidates that passed the η cut.

Jet definition

Jet is an object from an `ParticleJetContainer` with the StoreGate key *Cone4TowerParticleJets*, which satisfies:

1. Overlap removal with electrons: $dR(\text{electron}, \text{jet}) > 0.3$,
2. $|eta| < 2.5$,
3. $p_T > 25$ GeV.

Distributions of variables used in overlap removal are shown on Fig. 2, p_T and η cut variables on Fig. 3.

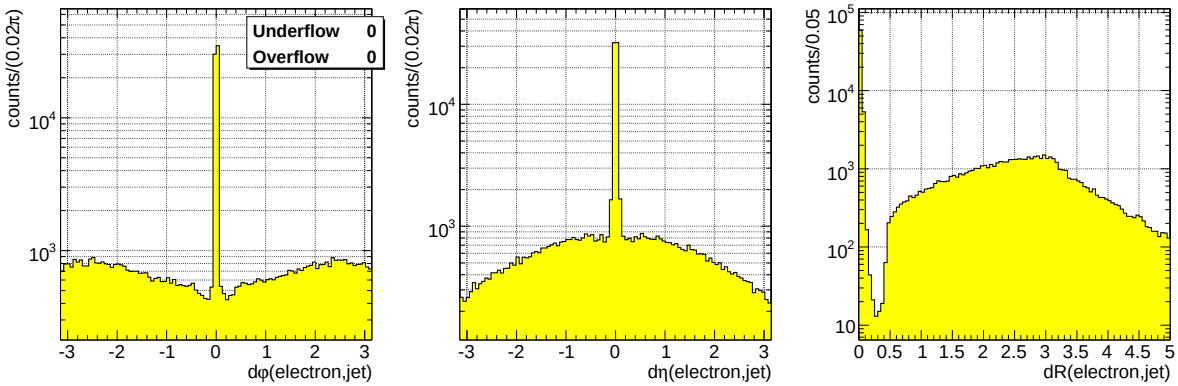

Figure 2: Distributions of jet-to-electron distances in η, φ, and R, in overlap removal.

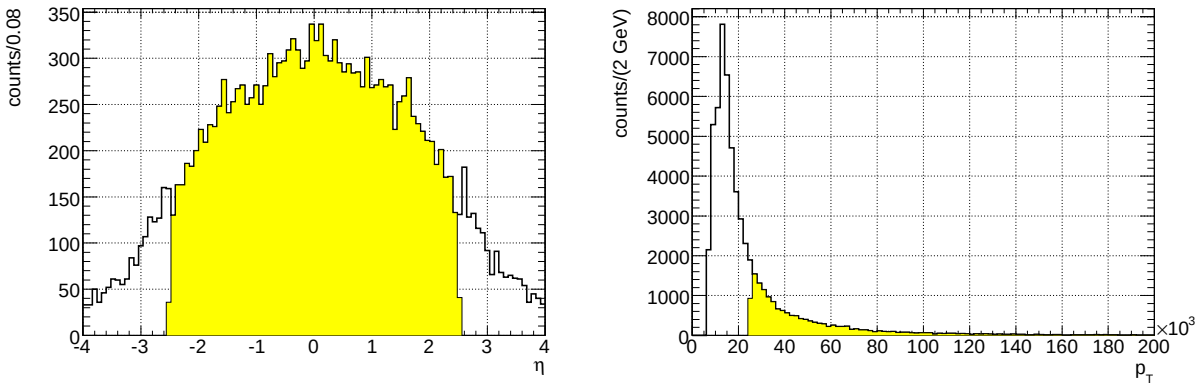

(a) (b)

Figure 3: Distributions of η (3(a)) and p_T (3(b)) of jet candidates. The η distribution includes only those the candidates that passed the p_T cut, and p_T distribution only the candidates that passed the η cut.

Event selection

Event selection cuts are designed to obtain an inclusive sample of $W^{\pm} \to e\nu$ events.

- Events are required to pass the L2e25i trigger.
- An event must have exactly one electron, as defined above. The 1 electron requirement was imposed in stages, as shown on Fig. 4. The event is said to fail the "electron author" cut if there are no AuthorEgamma electoron candidates in the input collection. Similarly, if there are no input electrons inside the accepted η or p_T range, or none passes the isEM requiremen, the event fails corresponding cut on Fig. 4.
- $\not{E}_T > 25$ GeV
- Transverse mass $m_t(\vec{p}_t(e), \vec{\not{E}}_T) > 45$ GeV
- In addition to the trigger bit requirement, we require that the reconstructed electron matches a trigger electron. This is necessary in order to be able to measure trigger efficiency using a tag and probe method.
- The final cut shown on Fig. 4, that requires a minimum of 4 jets, is used to define the $t\bar{t}$ event sample.

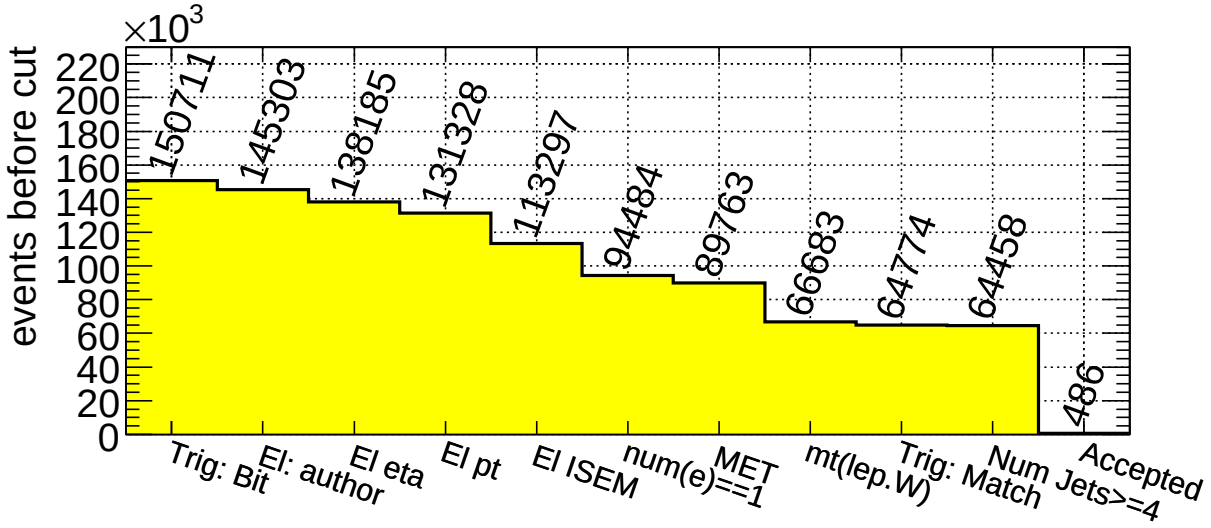

Figure 4: Number of events before each cut, on the streaming data set.

3 Calibrations and Efficiencies

3.1 Electron energy scale calibration

For electrons, we correct the electromagnetic energy scale of the release 12 simulation to agree with the scale observed in the streaming data. Before correction, a miscalibration is evident in the different shapes of the Z^0 mass peak in streaming data and in a PYTHIA $Z^0 \to e^+e^-$ sample[1)], as shown in Figure 5.

We assume that the effect of miscalibration can be represented by a factor which is independently a function of electron eta and energy, so the corrected energy can be written $E_{\text{corr}} = \alpha(\eta, E) \cdot E_{\text{sim}} \equiv \alpha_1(\eta)\alpha_2(E) \cdot E_{\text{sim}}$. We then determine the correction factor $\alpha(\eta, E)$ by calibrating the mean Z^0 mass in

[1)] We use `trig1_misal1_mc12.005144.PythiaZee.recon.AOD.v12000604`.

bins of η or E. The Z^0 mass squared reconstructed with corrected electron and positron energies in a given bin would be written $\alpha(\eta_+,E_+)\alpha(\eta_-,E_-)M^2_{\rm sim}$. To measure the correction, we simply equate this with the mean value of M_Z^2 from the streaming dataset.

In Figure 6, the average value of $(M_{Z^0})^2$ (scaled by the world average Z^0 mass squared) is plotted as a function of the lepton's energy and η for the streaming data and the release 12 simulation. The data distributions, proportional to $\alpha(\eta_p m,E_\pm)\langle\alpha(\eta_\mp,E_\mp)\rangle$ for positrons (electrons), have no discernable dependence on the charge of the lepton being averaged over. We combine the electron and positron plots to derive the calibration. The result is shown in Figure 7. The η and E distributions are consistent with a constant correction factor of 1.009 ± 0.001 in the range ($E > 25$) and ($0 < |\eta| < 1.3$ or $1.7 < |\eta| < 2.4$). We treat the variation of the correction in the cracks near $|\eta| = 1.5$ as a systematic errror.

We may incur a systematic bias by assuming that the correction is flat in electron energy. Allowing a linear term in the fit to $\alpha(E)$, the correction varies by $^{+0.002}_{-0.001}$ in the range 25 to 101 GeV (which encompasses 90% of the leading electrons in selected regions near the crack, ($1.3 < |\eta| < 1.7$), the derived correction shifts negligably by 0.004. We therefore combine a systematic error of 0.002 with the statistical error on the fit, so that the electromagnetic energy scale is known with a 0.22% relative systematic uncertainty.

3.2 Trigger Efficiency

We measure the electron trigger efficiency (with respect to reconstruction) of the L2_e25i trigger by applying the tag and probe method to electrons in the $Z \to ee$ peak. "Reconstructed" electrons are those that passed the cuts mentioned above **[they are mentioned above, right?]**, including all of the isEM cuts except possibly TRT. In events where there are two good electrons (of opposite charge) that give an invariant mass of $m_Z \pm 10$ GeV, we apply the standard tag and probe procedure and plot the trigger efficiency with respect to p_T and η in Fig. 8. Since the distribution is essentially flat for $p_T > 25$ GeV and for η outside the cracks, we quote an simple overall trigger efficiency rather than convoluting it with the p_T distribution of the electrons. **[Should I include a few more sentences and formulae on the "standard" tag and probe method?]**

There is one subtlety that arises from using simulated rather than real data. The definition of the L2_e25i trigger changed slightly between versions 11 and 12 of the ATLAS software. Since the streaming data were simulated with version 11 but reconstructed with version 12, the trigger decision for an electron need not agree with the decision of our (version 12) trigger cuts. Thus we define an `Electron` as triggered on if it matches, within a ΔR of 0.2, a `TrigElectron` that passes a set of cuts designed to match the version 12 trigger.

For electrons that pass our p_T and η cuts, we find the trigger efficiency with respect to reconstruction to be $\varepsilon_t = (98.96 \pm 0.11)\%$. The error quoted is statistical; the systematic error is negligible. The primary background to events passing our Z mass window cut are W and top events with two good electrons, and the properties of such electrons should be identical to those of $Z \to ee$ electrons as far as the trigger is concerned.

3.3 Missing transverse energy scale

3.3.1 Uncertainty in the $\not{E}_T$ scale

The missing transverse energy used to select $W^\pm$ candidates in this analysis is calculated from a sum over specifically calibrated calorimeter cells in three categories: cells in electromatic clusters, in jets, and in clusters not associated with any reconstructed calorimeter object [1]. This sum is then corrected for the E_T of identified muon candidates and for probable energy loss in the cryostat. Since the cell energies

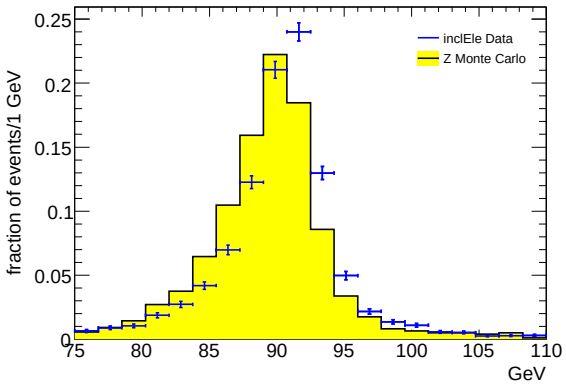

Figure 5: Differences in the electron energy scale in streaming data and the release 12 simulation sample lead to a systematically shifted reconstructed Z^0 mass.

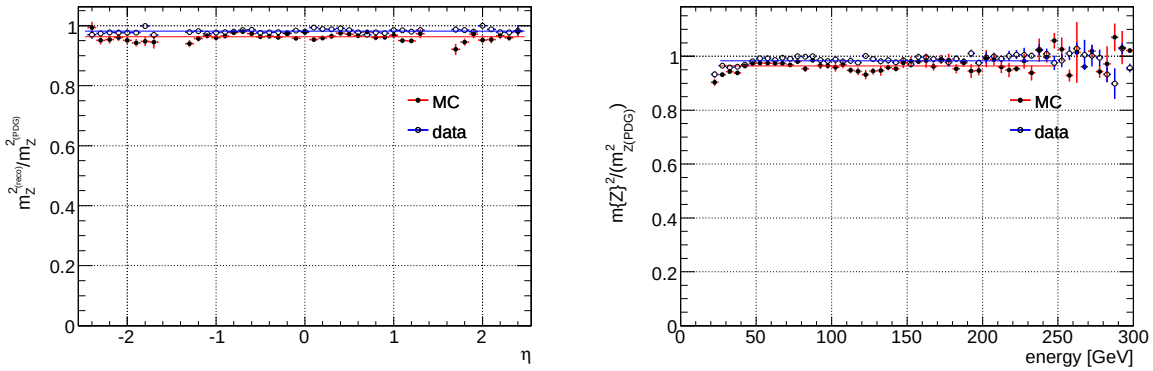

(a) Average Z^0 mass squared, scaled by $M^2_{Z^0}(PDG)$, *vs.* electron/positron η.

(b) Average Z^0 mass squared, scaled by $M^2_{Z^0}(PDG)$, *vs.* electron/positron E.

Figure 6: Dependence on lepton kinematics of the reconstructed Z^0 mass in streaming data and release 12 PYTHIA Monte Carlo.

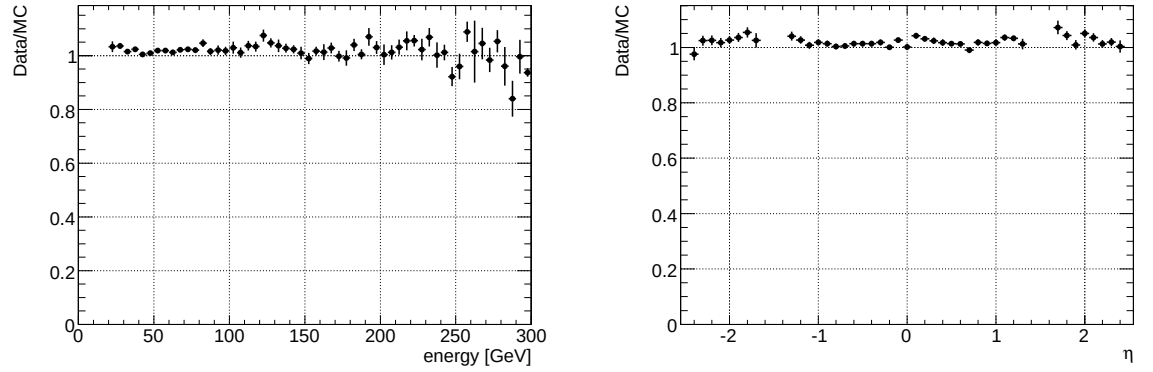

(a) Derived energy correction as a function of electron η.

(b) Derived energy correction as a function of electron E.

Figure 7: Correction to the electron energy required for the release 12 simulation.

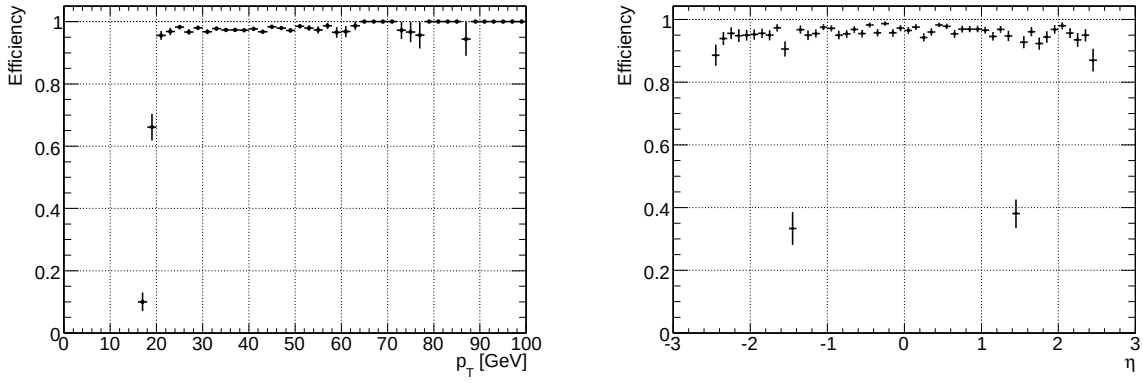

(a) (b)

Figure 8: The trigger efficiency for electrons from Zs, as a function of electron p_T (a) and of electron η (b). These plots are made before the p_T or η cuts are applied.

recieve either electromagnetic or hadronic energy scale corrections, a systematic miscalibration of the $\not\!\!E_T$ could result from miscalibrations of either scale, or of the muon identification efficiency.

As a first comparison of the scale of missing energy measurements in the release 12 simulation and the streaming data, we analyze the $W^{\pm}$ transverse mass distribution. This distribution is unaffected by differences in the $W^{\pm}$ boson kinematics, but other sources of true missing energy such as additional neutrinos or unidentified muons, will disort this distribution in the streaming data. We use the $t\bar{t}$ preselection (**let's define this upstream.** the lepton selecton with the requirement that only one tight lepton is found in the event, and the missing energy cut of 25 GeV) to select $W^{\pm}$ candidate events in the streaming data and a PYTHIA $W \to e\nu$ sample[2)] simulated in release 12.0.6. We apply the lepton energy scale correction derived in section 3.1 and subtract the change in the electron's transverse momentum vector from the missing energy. By requiring that the multiplicity of jets with p_T greater than 25 GeV be less than 2, we exclude most $t\bar{t}$ and other background events. The $W^{\pm}$ transverse mass reconstructed in each sample is plotted in Figure 9. The ratio between the mean $m_T(W)$ in the streaming data and the PYTHIA sample is 1.019 ± 0.001 when $N_{\text{jets}} = 0$ and 1.011 ± 0.003 when $N_{\text{jets}} = 1$.

3.3.2 Systematic uncertainty in the signal acceptance due to $\not\!\!E_T$ calibrations

This section should move to systematics. The study in Section 3.3.1 indicates a systematic uncertainty of about 3% for low jet multiplicities. However, the method is too sensitive to contamination by $t\bar{t}$ events to be used in the high jet multiplicity region, and comparision of the ratios determined in the 0- and 1-jet bins does not rule out a correlation with jet activity. To estimate a systematic uncertainty, we simply assume that the jet energy scale miscalibration is the dominant driver of the missing energy scale in events with a large jet multiplicity. We therefore assign the $\not\!\!E_T$ scale the same nominal 5% uncertainty as the jet energy scale. We then calculate the effect of such an uncertainty on the signal acceptance.

[2)] We use `trig1_misal1_csc11.005100.JimmyWenu.recon.AOD.v12000601`, applying the "1mm" bug correction in the AOD [2].

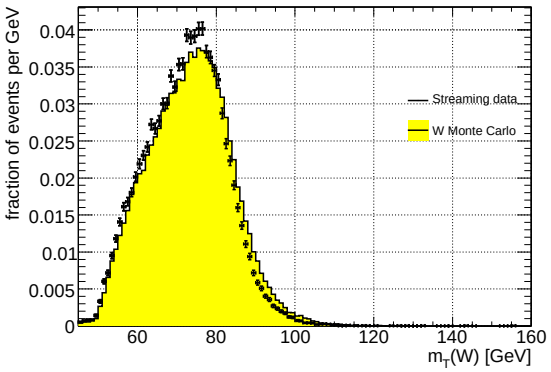

(a) $W^{\pm}$ transverse mass for events with $N_{\text{jets}} = 0$.

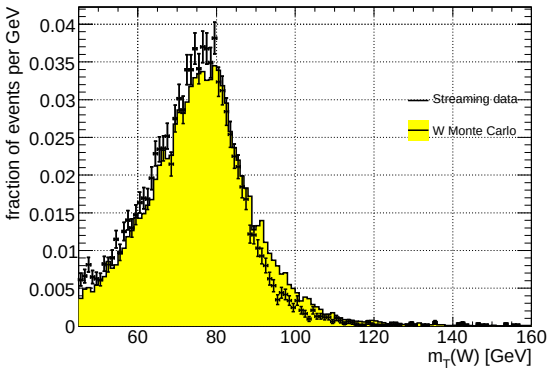

(b) $W^{\pm}$ transverse mass for events with $N_{\text{jets}} = 1$.

Figure 9: Studies of $m_T(W)$ and $\not\!\!E_T$ scale in streaming data and the release 12 simulation.

Missing E_T scale	**Lepton+jets acceptance**	**relative change**
1.05	0.054 ± 0.01	+4%
0.95	0.050 ± 0.001	-4%

Table 1: The acceptance of our event selection (excluding trigger requirements) with different missing energy scale settings.

4 Signal Acceptance

4.1 Acceptance

In this section we summarize the acceptance of our event selection for $t\bar{t}$ signal events generated with MC@NLO. The MC@NLOsample used was created with a generator-level filter requiring a lepton with $p_T > 5$ MeV, so in this note we refer to efficiencies with respect to this $t\bar{t}$ inclusive lepton sample. The efficiency of our event preselection for $t\bar{t}$ leptonic events is **presel** and the final efficiency, which includes the jet multiplicity cut, is 5.3ish $\pm$ 0.something %, where the errors quoted are statistical. We explore systematic errors on the signal acceptance in Section 7.1.

Event selection requirement	**acceptance (relative to previous cut)**
Generator filter (single lepton, $p_T > 5$ MeV)	0.554 ± 0
electron electron $p_T \geq 25$ GeV electron is unique $\not\!\!E_T \geq 25$ GeV $W^{\pm}$ $m_T > 45$ GeV	
$N_{\text{jets}} \geq 4$	

Table 2: The acceptance of our event selection (excluding trigger requirements) for signal events.

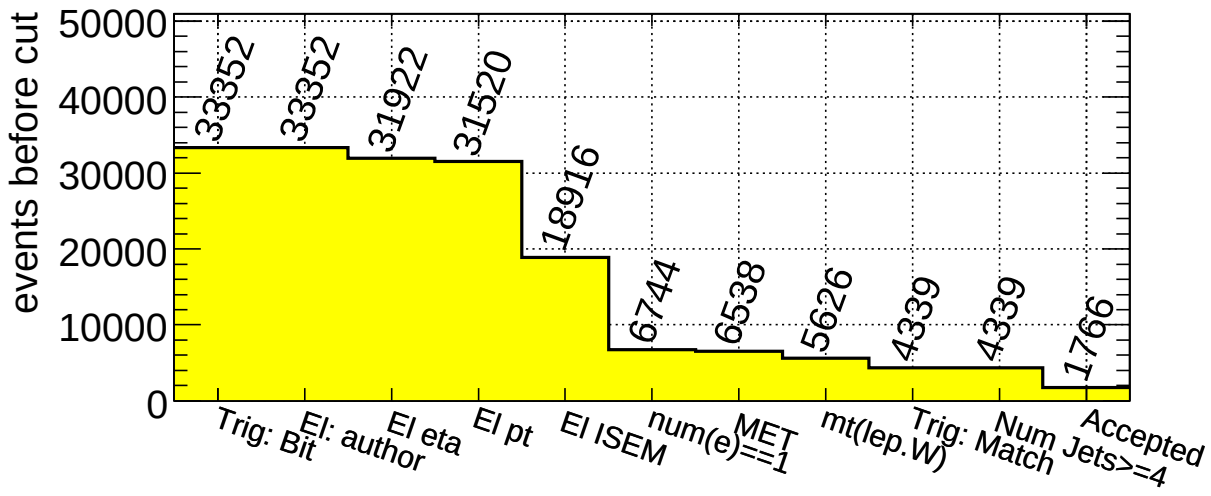

Figure 10: Graphical representation of the effect of sequential cuts on the number of events in the 005200.T1_McAtNlo_Jimmy dataset.

5 Backgrounds

5.1 Electroweak backgrounds

* W+jets: — now this is 'Electroweak' Andrei Plots and Tables and Text

** Normalization (e.g. cross section) W Cross Section Cross Check MDS must subtract Z and Tau cross section

** acceptance (after corrections) Andrei Cut plots

5.2 Single top

* Single top — just added Have plots with Default MC (ACER) Need to think about systematics

5.3 Fake electrons

In real data, we anticipate that jets sufficiently electron-like to trigger on will be a substantial background. However, since jet rejection is of the order 10^3, simulating a large number of these fake electrons is computationally prohibitive. Thus they do not exist in the streaming data. To verify that this background is negligible, we plot the distributions of the electron identification variables used in setting the isEM flags. See Fig. 11 for example plots. [To be added to!]

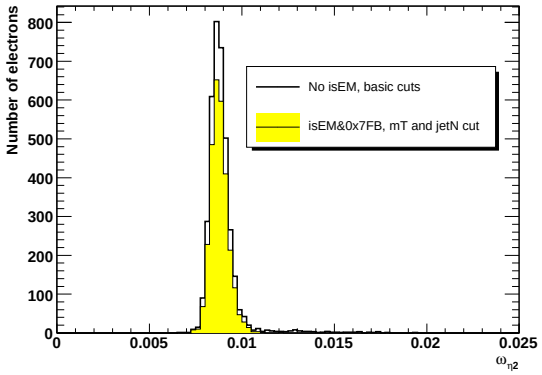

(a) The variable $\omega_{\eta 2}$, a measure of shower width in η in the second sampling of the electromagnetic calorimeter.

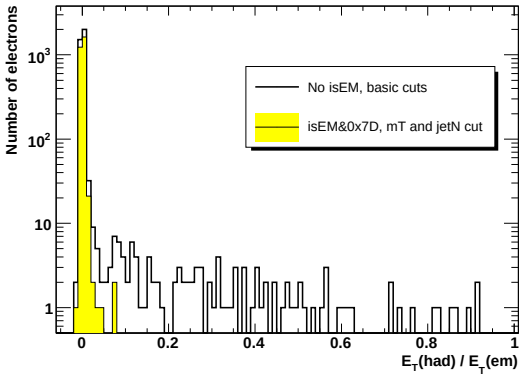

(b) Hadronic leakage, the ratio of energy in the hadronic calorimeter to energy in the electromagnetic calorimeter.

Figure 11: Examples of electron ID events. **[My use of yellow/unfilled has a different meaning than the use above. Is that confusing?]**

Generator	acceptance
AcerMC	0.0580 ± 0.06
MC@NLO	$0.0524 \pm$
Pythia	0.0534 ± 0.3

Table 3: The acceptance of our event selection (excluding trigger requirements) for events generated with MC@NLO, AcerMC, and Pythia .

6 Cross section or Method or whatever

6.1 Without fit method

6.2 Fit method

7 Systematic uncertainties

7.1 Signal modeling systematics

7.1.1 Monte Carlo Generator

We use MC@NLO [3] version 3.1, with Jimmy [4] showering, to generate the $t\bar{t}$ signal events and determine our acceptance. This generator includes all terms in the matrix element up to order α_s^3, but neglects some observable angular correlations. As a very crude estimate of the theoretical uncertainty, we compare the acceptance calculated above to the acceptance derived with AcerMC, which uses a leading-order calculation of the $t\bar{t}$ production matrix elements combined with Pythia showering, and with Pythia alone.

7.1.2 Initial and final state radiation

Uncertainty in the modeling of initial and final state radiation affects the average number of jets above threshold in top events, and thus the acceptance of our event selection (especially the final $N_{\text{jet}} > 3$

Sample	PYTHIA settings	acceptance
AcerMC "low m_T"	PARP(81,61,62) *= 2,0.5,2,0.5	9.3
AcerMC "high m_T"	PARP(81,61,62) *= 0.5,2.0.5	7.8

Table 4: Signal acceptance (from ATLFAST) in ISR/FSR systematic samples. **this clearly needs formatting and clarification**

requirement). Here, we compare the signal acceptance calculated using three alternative Pythia settings.

* changing the parp81 from 1.9 GeV: NJ decreases as par increases. jet to quark energy decreases. parp62? lambdaQCD higher: more jets, more top PT. Hence changes preserve NJ somewhat but make jets less energetic.

The acceptance was calculated using ATLFAST rather than fully reconstructed samples.

** Systematics: 1-2 jet comparison Big Discussion Still underway: Joe, Peter, Andrei and Andre

Z vs W. Can use Z in higher Nj bins to estimate the background without being affected by ttbar. But need W/Z ratio and systematic on it.

8 Results

As noted above, we observe 486 ttbar candidate events in the 14.81 pb^{-1} of good luminosity blocks in the streaming data.

** summary of systematic errors Review of above (Table)

* Cross section, given "all-top" hypothesis Andrei

9 Future refinements

9.1 Refinement of Analysis

9.1.1 b-Tagging

Identifying jets from b-quark fragmentation is not necessary for isolating $t\bar{t}$ event candidates, however it is useful for calibrations and cross-checks. In this analysis we use the current default tagger 1P3D+SV1 (reference?) which is a combination of a 3D impact parameter tagger and a secondary vertex tagger. A jet is defined to be tagged as a b-jet if its weight is greater than 3.0.

Jet multiplicity distributions for events passing the preselection cuts are plotted in Fig. 12 for streaming data and for the MC@NLO $t\bar{t}$ sample without b-tagging and when requiring at least one respectively at least two b-jets. Fig. 13 shows the sample composition of events with at least one or at two b-jets. The PYTHIA electroweak background samples $W \to e\nu$, $W \to \tau\nu$ and $Z \to ee$ are, after normalization to their relative cross sections, scaled to match the number of events in the (0+1) jet bins for the streaming data without requiring b-tagging and this scale factor is then applied to the samples when using b-tagging. The $t\bar{t}$ sample and the ACERMC single top samples are all normalized according to their cross sections.

9.1.2 Di-Lepton Mode

1/9 of $t\bar{t}$ decays are fully leptonic with both $W^{\pm}$ decaying into a lepton and a neutrino. The di-lepton mode provides a clean sample and is despite its limited use in reconstructing the top mass valuable for cross-checks with results from the semi-leptonic mode and for providing a $t\bar{t}$ subsample with highly reduced background.

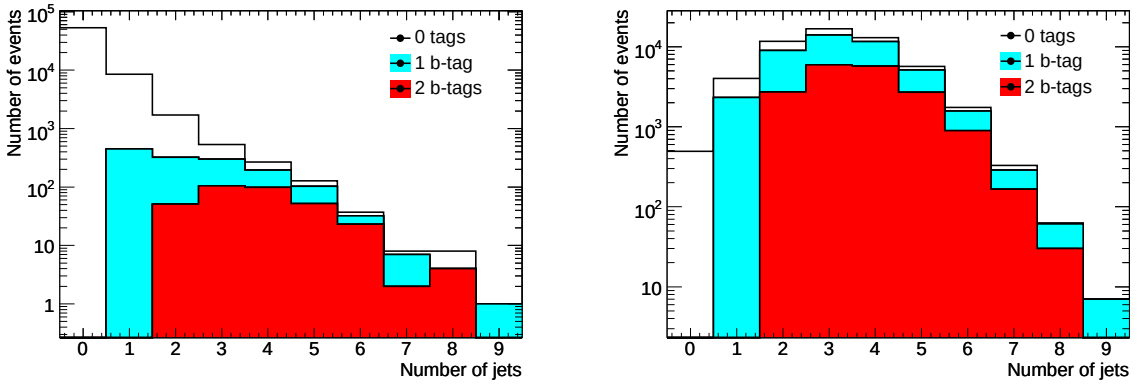

(a) (b)

Figure 12: Jet multiplicity distributions for streaming data (12(a)) and the MC@NLO $t\bar{t}$ sample (12(b)) for semi-leptonically decaying events with zero, at least one or at least two b-tagged jets.

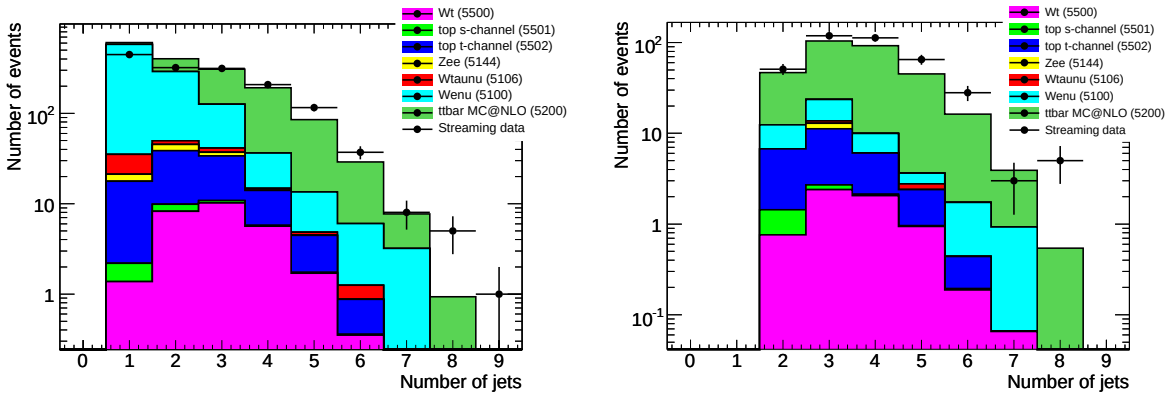

(a) (b)

Figure 13: Normalized jet multiplicities for streaming data and its different components when requiring at least one (13(a)) or at least two b-jets (13(b)) for the semi-leptonic mode.

For the dilepton mode we select events with exactly one electron (as defined in section 2.1) and exactly one muon. A muon is defined as an object from a `MuonContainer` with the StoreGate key *MuidMuonCollection* and for which:

1. $p_T > 15$ GeV
2. $|\eta| < 2.4$
3. isolation $E_T < 6$ GeV in a cone of 0.2
4. $dR(\mu, jet) > 0.3$

For these events, jet multiplicity distributions with and without requiring b-tagging are shown in Fig. 14 for streaming data and MC@NLO $t\bar{t}$. Similarly to the semi-leptonic case, jet multiplicities are plotted for fully leptonic event candidates to show the sample composition without b-tagging (Fig. 15) and with at one or two b-jets (Fig. 16). For the di-lepton mode we include a PYTHIA $W \rightarrow \mu\nu$ sample in the electroweak background in addition to the ones used for the semi-leptonic mode. (Fig. 16) only includes the background samples which had any contributions to the jet multiplicites after normalization.

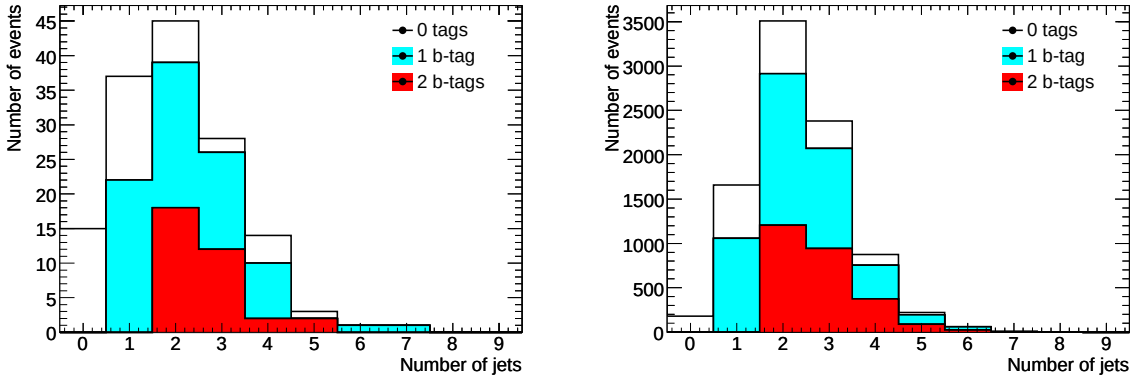

(a) (b)

Figure 14: Jet multiplicities for streaming data (14(a)) and MC@NLO $t\bar{t}$ (14(b)) for events in the di-lepton mode without b-tagging and with at least one or two b-tagged jets.

9.1.3 Reconstructed Top Mass

To validate the $t\bar{t}$ event selection for the semi-leptonic mode we consider the invariant mass of the hadronically decaying $W^{\pm}$ and corresponding reconstructed top mass. We isolate events with four or five jets of which two are tagged as b-jets. For events with four jets, the hadronic $W^{\pm}$ mass is calculated from the two untagged jets. For events with five jets there are three possible combinations of the $W^{\pm}$ mass and for these we choose to have three entries per event. The distribution of the invariant mass is shown in Fig. 17 for streaming data and MC@NLO $t\bar{t}$ respectively.

The reconstructed top mass is determined by choosing the three-jet combination of the di-jets constituting the hadronic $W^{\pm}$ together with the b-jet resulting in highest total transverse momentum. As for the $W^{\pm}$ invariant mass we have one entry per event for the four-jet bin and three entries per event for the five-jet bin. The distribution of the reconstructed top mass is shown in Fig. 18 for streaming data and MC@NLO $t\bar{t}$.

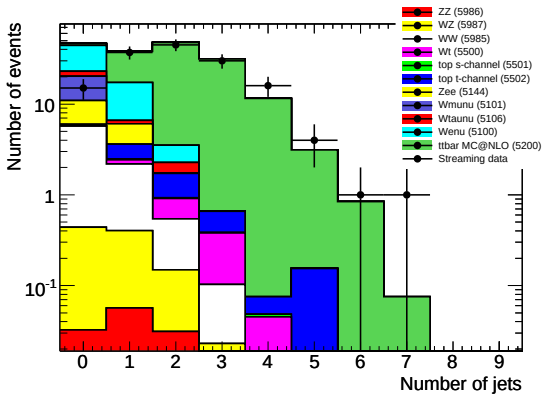

Figure 15: Normalized jet multiplicities for streaming data and its different components without b-tagging for fully leptonic event candidates.

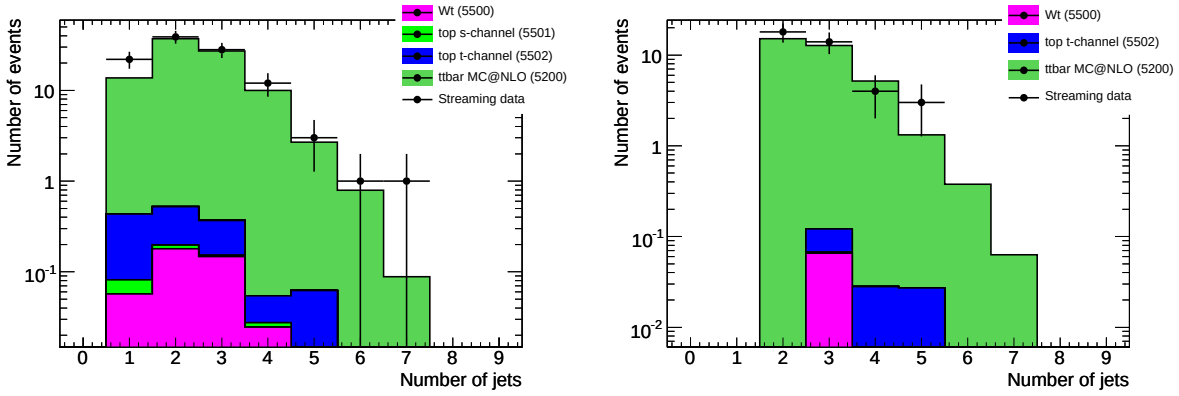

(a) (b)

Figure 16: Normalized jet multiplicities for streaming data and its different components when requiring at least one (16(a)) or at least two b-jets (16(b)) in the di-lepton mode.

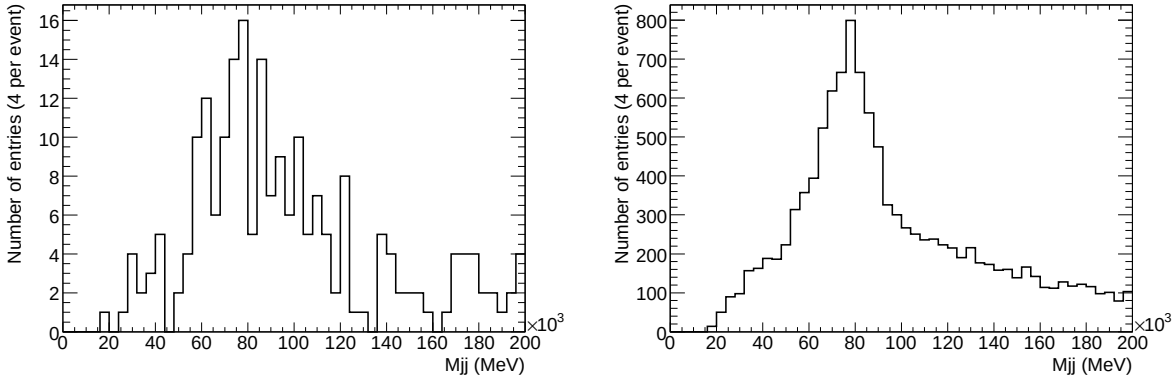

(a) (b)

Figure 17: Invariant mass of the hadronic $W^{\pm}$ for streaming data (17(a)) and MC@NLO $t\bar{t}$ (17(b)) for events with four or five jets of which two are b-tagged.

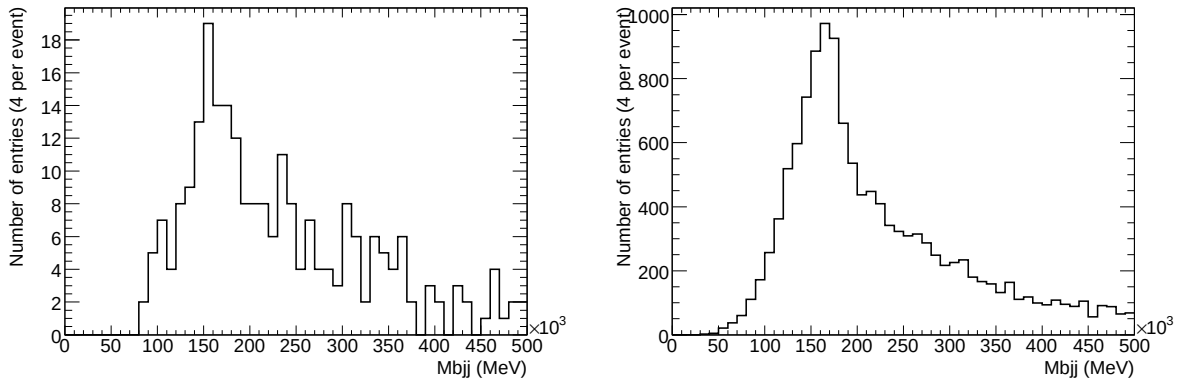

(a) (b)

Figure 18: Reconstructed top mass for events with four or five jets of which two are b-tagged for streaming data (18(a)) and MC@NLO $t\bar{t}$ (18(b)). For each hadronic $W^{\pm}$ di-jet combination, the three-jet combination (two untagged jets plus one b-jet) resulting in highest sum p_T is chosen.

10 Acknowledgements

References

[1] S.L. Glashow, Nucl. Phys. **22** (1961) 579.

[2] ”NewsForPhysicsUsers, https://twiki.cern.ch/twiki/bin/view/Atlas/NewsForPhysicsUsers”.

[3] S. Frixione and B. R. Webber, (2002).

[4] G. Corcella and I. G. Knowles and G. Marchesini and S. Moretti and K. Odagiri and P. Richardson and M. H. Seymour and B. R. Webber, JHEP **0101** (2001) 010.